Article

J. Biol. Regul. Homeost. Agents. 2024; 38(5): 4439–4452
https://doi.org/10.23812/j.biol.regul.homeost.agents.20243805.353

Identification of m^{7}G-related Subtypes, Validation of Prognostic Models, and Tumor Immune Microenvironment in Gastric Cancer

Yongjian Lin[1,†], Shenyi Lu[2,†], Wenqian Xu[1], Jinlu Liu[1,*]

[1]Department of Gastrointestinal and Gland Surgery, The First Affiliated Hospital of Guangxi Medical University, 530021 Nanning, Guangxi, China
[2]Department of Rehabilitation, The Affiliated Hospital of Youjiang Medical University for Nationalities, 533000 Baise, Guangxi, China
*Correspondence: liujinlugx@163.com (Jinlu Liu)
[†]These authors contributed equally.
Published: 1 May 2024

Background: Gastric cancer (GC) ranks as the fourth most prevalent cancer globally, with heterogeneous prognosis and high mortality rates. Numerous studies have highlighted the close association between the occurrence and progression of gastric cancer and the N7-methylguanosine (m^{7}G) mechanism. This study aims to determine the clinical significance of m^{7}G-related genes (m^{7}Gs) in gastric cancer prognosis and investigate their potential connection with the tumor immune microenvironment (TIME).

Methods: Gastric cancer data was obtained from the Cancer Genome Atlas (TCGA) library to generate the m^{7}G pattern prognosis-related genes (m^{7}G-PRGs) matrix. Two distinct m^{7}G typings were initially identified, followed by unsupervised clustering based on m^{7}G-related cluster C1 and C2 (m^{7}G-C1/2) integrated differentially expressed genes (DEGs) to acquire a scoring system. The m^{7}G-related prognostic model (m^{7}G-RPM) was then constructed, with key prognostic genes experimentally validated through Western blot analysis. Subsequently, gastric cancer patients were stratified into high/low-scoring subgroups using the calculated median m^{7}G_score, facilitating the investigation of prognosis-related mechanisms. Furthermore, biological signaling pathways were systematically enriched, a nomogram was developed, and TIME in gastric cancer was assessed.

Results: Alterations in m^{7}Gs are associated with a poor prognosis, with the primary outcome being hypermethylation in cancer, which regulates immune signaling and promotes cellular infiltration. Two distinct m^{7}G clusters were identified, revealing m^{7}Gs' bidirectional regulatory role in clinicopathological features and the TIME. A nomogram containing seven variable genes improved the clinical applicability of m^{7}G-RPM, with increased solute carrier family 39 member 4 (*SLC39A4*) and matrix metallopeptidase 7 (*MMP7*) expression observed in gastric cancer cells. The m^{7}G_score was significantly associated with microsatellite instability (MSI), tumor mutation burden (TMB), chemotherapeutic drug sensitivity, and cancer stem cell (CSC) index.

Conclusion: A comprehensive analysis of m^{7}G s in gastric cancer confirmed their potential role in genetic alterations, TIME, clinical traits, and prognosis, especially in tumor-infiltrating immune cells (TIICs). We constructed a novel prognostic model based on m^{7}Gs and performed preliminary validation of the screened genes. These findings present innovative perspectives for assessing the prognosis of gastric cancer and guiding individualized immunotherapy strategies for patients.

Keywords: N7-methylguanosine; gastric cancer; prognosis; tumor immune microenvironment; treatment

Introduction

Gastric cancer (GC) patients are ranked fourth in the world, with both low early diagnosis and cure rates contributing to an inferior 5-year survival rate. The standard surgery for GC combining limited lymph node dissection is believed to be the only radical strategy. However, heterogeneous GC prognoses remain, including lymph node metastasis, peritoneal spread, and significant drug resistance. Zhai *et al.* [1] reported that methylation-modified eukaryotic translation initiation factor 4E binding protein 3 (*eIF4EBP3*) was downregulated and functioned as a tumor suppressor in GC by targeting the eukaryotic translation initiation factor 4E (*eIF4E*)/β-linked protein axis. *eIF4E* and methylation-associated novel tumor suppressor genes (TSGs) could inhibit the proliferation and metastasis of GC cells, suggesting the presence of prognostic biomarkers within the methylation gene family for GC.

Advances in sequencing technology have extended the scope of gene regulatory processes to the neo-level, including RNA modifications such as pseudouridylation (Ψ), N6-methyladenosine (m^{6}A), and N7-methylguanosine (m^{7}G). Cumulative studies have demonstrated that the oncogenic effect of m^{7}G is beneficial to improving the therapeutic efficacy and prognosis of cancer [2]. For example, endogenous N-methylguanosine in tumors improves anti-PD-1 efficacy, suggesting m^{7}G-based mechanisms as a strategy for combined immunotherapy [3]. Alternatively, dysregulation

Journal of
BIOLOGICAL REGULATORS
and Homeostatic Agents

of m^7G methylation occurs in tumor progression and therapeutic response, exemplified by the cooperative action of coenzyme *METTLE1* and WD repeat domain 4 (*WDR4*) in promoting cell proliferation and treatment [4]. Therefore, the regulation of m^7G-related genes is crucial for the investigation of GC, with potential implications on immunotherapy.

Beyond its role in cellular metabolism, stabilization, exonucleation, and protein translation, m^7G is intimately associated with chemoresistance, antitumor, and metastasis in GC. The knockdown of pro-apoptotic protein cytoplasmic FMR1 interacting protein 2 (*CYFIP2*) activates the Protein Kinase B (*Akt*)-pro survival signaling pathway to develop chemotherapy resistance in cancer cells. *CYFIP2* knockdown is an effective anti-GC therapy that inhibits the downstream pathway of m^7G-related genes (m^7Gs) in combination with chemotherapeutic drugs *in vivo* [5]. Tan *et al*. [6] reported that silencing *NUDT5* in GC cells inhibits *Akt*/GSK-3β/β-catenin, which is associated with chemotherapy sensitivity. Additionally, the miR-485-5p/nudix hydrolase 1 (*NUDT1*) axis is involved in key processes of tumor cell growth and motility. High intra-tumor *eIF4A1* expression promotes epithelial-mesenchymal transition, predicting a worse prognosis in GC [7]. He *et al*. [8] observed an upregulated *eIF3d* expression in GC tissues, correlating with lymph node metastasis and depth of infiltration. *NUDT10* overexpression is associated with advanced GC clinicopathological features and a poorer prognosis, suggesting its potential as a prognostic marker [9]. Several genes exhibit diverse functions, such as SUMO-2/3-modified NOP2/Sun RNA methyltransferase 2 (*NSUN2*), which simultaneously regulates mRNA C5-methylcytidine (m5C) and promotes GC progression [10]. Therefore, investigating the polygene-mediated m^7G-related mode would help predict GC prognosis and understand the mechanisms underlying tumor progression.

In general, the tumor microenvironment (TME) serves as the "soil" of cancer cells, where GC progression, metastasis, and drug resistance occur, and involves crosstalk between immune infiltrating cells. On the one hand, the knockdown of m^7Gs in cancer cells not only alters the tumor immune microenvironment (TIME) and stromal compartment [11] but also enables resistance to immunologically hot phenotypes by evading recognition from the immune surveillance system, including cytotoxic T lymphocytes (CTLs), natural killer (NK) cells, macrophages, and other components of antitumor immunity. Conversely, the immunologically cold phenotype of the TIME differential theory is strongly linked to immune negative indicators in lung adenocarcinoma, such as *EGFR/SRGN* and immune checkpoint inhibitors (ICIs) [12]. The m^7G-modified tumor-infiltrating immune cells (TIICs) might indicate TME remodeling and bipolarity, correlating with clinical outcomes. Based on the methylation effect potentially providing an accurate prognosis for GC patients, and the existence of response genes related to immunotherapeutic sensitivity in GC tissues, both may be essential elements of precise cancer treatment.

While numerous studies have addressed the development of prognostic models related to gastric cancer (GC), those specifically involving m^7Gs have been limited. Resultantly, our study comprehensively evaluated m^7Gs expression profiles and obtained an overview of immune landscapes within GC using both the CIBERSORT and ESTIMATE algorithms. Based on the expression levels of m^7Gs, 808 GC patients were randomly clustered into two independent subtypes, from which we obtained related biological pathways. After pathway enrichment, this study focused on the effects of m^7Gs on TIICs and cell functions. Furthermore, we developed the m^7G-related prognostic model (m^7G-RPM) to effectively predict overall survival. Further analyses, including nomogram and clinical composite index assessments, improved the clinical applicability. Finally, this study offers novel insights into the mechanism of m^7G regulation in epigenetics by analyzing TME and drug sensitivity in gastric cancer.

Materials and Methods

Acquisition of Raw Data

The gene sequencing matrix and comprehensive clinicopathology files of GC patients were derived from the Cancer Genome Atlas (TCGA, https://www.cancer.gov/about-nci/organization/ccg/research/structural-genomics/tcga) and the Gene Expression Omnibus (GEO, https://www.ncbi.nlm.nih.gov/gds/) online databases. The research utilized the stomach adenocarcinoma (STAD) cohort as the training set, and the GSE84437 set as the validation set. After removing duplicates and samples lacking prognostic features, 808 GC samples and 32 normal samples were included in this study. The m^7Gs were obtained from previously studied and reported literature [13]. The integration, transformation of Transcripts Per Million (TPM), and differential gene expression analysis were conducted using the "limma" R package (Version 3.42.2). Moreover, we eliminated the batch effect of TPM to minimize the impact of technical differences on the results.

Genetic Variation and Molecular Biology

The somatic mutation data, including proto-oncogene KRAS and BRAF point mutations, as well as copy number variation (CNV) data were accessed from TCGA. Waterfall plots were used to illustrate various types of mutations. CNVs within m^7Gs and the genomic locations of CNV alterations on chromosomes were respectively visualized using a bar graph and a Circos plot. The associated annotation files "c2.cp.kegg.v7.4.symbols" and human gene annotation files generally utilized for gene set enrichment analysis were loaded from the MSigDB database

(https://www.gsea-msigdb.org/gsea/login.jsp) and ensemble website (https://asia.ensembl.org/index.html), respectively. Gene set variation analysis (GSVA), a special type of gene set enrichment method [14], focused on the major pathways associated with m^7Gs. The Kyoto Encyclopedia of Genes and Genomes (KEGG) enrichment results were then visualized using a heatmap.

Co-clustering Analysis of m^7Gs and ssGSEA

The core genes of the m^7Gs interaction network and the associated favorable factors were identified via Cox analysis. Utilizing the "ConsensusClusterPlus" R package (Version 1.54.0), the matrix of 34 m^7Gs expression obtained from the merged set was identified and clustered without supervision. This study utilized the following parameters: The cumulative distribution function (CDF) was increased smoothly and the proportion of items to sample (pItem) was set to 80%. The hierarchical clustering method was "km", with k = 2 as the optimal matrix used to find the novel m^7G subtypes. Following the initial clustering, two groups of distinct m^7G-related clusters, C1 and C2, were obtained. Single sample gene set enrichment analysis (ssGSEA) was used to estimate the relative abundance of immune cell types [15]. By comparing the gene expression data of each sample with the immune cell gene set, we could estimate the relative enrichment of the m^7G gene set in GC.

Immune Infiltration Analysis with the TME Landscape

The CIBERSORT method was used to quantify the abundance of each immune cell type in GC patients and assess tumor immune infiltration [16]. Following the comparison of immune infiltration between the C1 and C2 subgroups using CIBERSORT, we employed the "ggplot2" package (version 3.4.4, Systat Software and University of Illinois at Chicago, Chicago, IL, USA) to visually represent the proportional distribution of 22 immune cell types. Spearman correlation analysis was used to evaluate the strength and direction of the relationship between cell proportions and m^7Gs. The results of the correlation analysis and "ggplot2" were combined to create marginal scatter diagrams.

Relationship between Molecular Subtypes and Clinicopathological Features of GC

To assess the clinical value of the m^7G subtypes, we compared the clinicopathological characteristics and follow-up data between the two clusters. Clinical variables include age, sex, Tumor Node Metastasis (TNM) stage, overall survival, and status, with projects from both the TCGA cohort and the GEO dataset. Distinguishable dimensions of different m^7G subtypes were delineated using principal component analysis (PCA). Survival analysis and Kaplan-Meier (K-M) curves were conducted using the "survival" and "survminer" R packages (Version 3.2.7, University of Auckland, Auckland, New Zealand).

LASSO Algorithm to Quantify Methylation Patterns

To generate the m^7G-associated prognostic genes, crossover genes were extracted from differentially expressed genes (DEGs), and subsequent univariate Cox regression analysis was performed. Prognostic DEGs with $p < 0.05$ in the univariate Cox regression analysis were then clustered identically. Using the least absolute shrinkage and selection operator (LASSO) algorithm, the λ_{min} was selected after 10-fold cross-validation through the "glmnet" package (Version 4.1.2) to construct a scoring system. Subsequently, the optimal risk prediction model was established via multifactorial Cox regression analysis. The model risk scores were calculated as follows: $m^7G\_score = \sum_1^n Coef(mRNAn) \times Expr(mRNAn)$, where Coef(mRNAn) represents the coefficient and Expr(mRNAn) denotes the expression of the selected m^7Gs. We then integrated clinical characteristics (including age, gender, and TNM stage) into m^7G-RPM and constructed a nomogram with the "Regplot" R package (Version 1.1). Finally, the model's accuracy was validated through calibration and receiver operating characteristic (ROC) curves.

Western Blot and m^7Gs Expression in GC

Total proteins were extracted from human normal gastric epithelial cells lines (GES-1; iCell-h062, iCell Bioscience, Shanghai, China) and the human gastric cancer cells lines (AGS; CC-0401, Cellcook, Guangzhou, China) using RIPA lysis buffer (P0013B, Shanghai Biyuntian Biotechnology Co., Ltd., Shanghai, China). Cells were tested for mycoplasma and STR identification. The BCA Protein Assay Kit (ZJ101, Shanghai Ya Mei Biopharmaceutical Technology Co., Ltd., Shanghai, China) was utilized to quantify the proteins. The proteins in each sample were separated by Sodium dodecyl-sulfate polyacrylamide gel electrophoresis (SDS-PAGE) and transferred to the nitrocellulose filter membranes. Subsequently, the membranes were incubated overnight at room temperature in 5% nonfat milk/TBST buffer. The primary antibody was incubated with solute carrier family 39 member 4 (*SLC39A4*) Polyclonal Antibody, Beta-Actin Polyclonal Antibody, matrix metallopeptidase 7 (*MMP7*) Polyclonal Antibody, and *GADPH* Polyclonal Antibody, respectively. The membrane complexes were then incubated overnight with Goat anti-Mouse Poly-HRP Secondary Antibody and Goat anti-Rabbit Poly-HRP Secondary Antibody (PR30012 and PR30011, Wuhan Sanying Biotechnology Co., Ltd., Wuhan, China). Finally, the obtained immune complexes were analyzed using Image-Pro Plus software (Version 6.0, Media Cybernetics, Bethesda, MD, USA). Based on the Human Protein Atlas (HPA) database (https://www.proteinatlas.org/), we assessed the expression and protein sublocalization of key proteins in six sets of GC samples. After comparing the approximate expression levels of Solute carrier family 27 member 2 (*SLC27A2*),

Journal of
BIOLOGICAL REGULATORS
and Homeostatic Agents

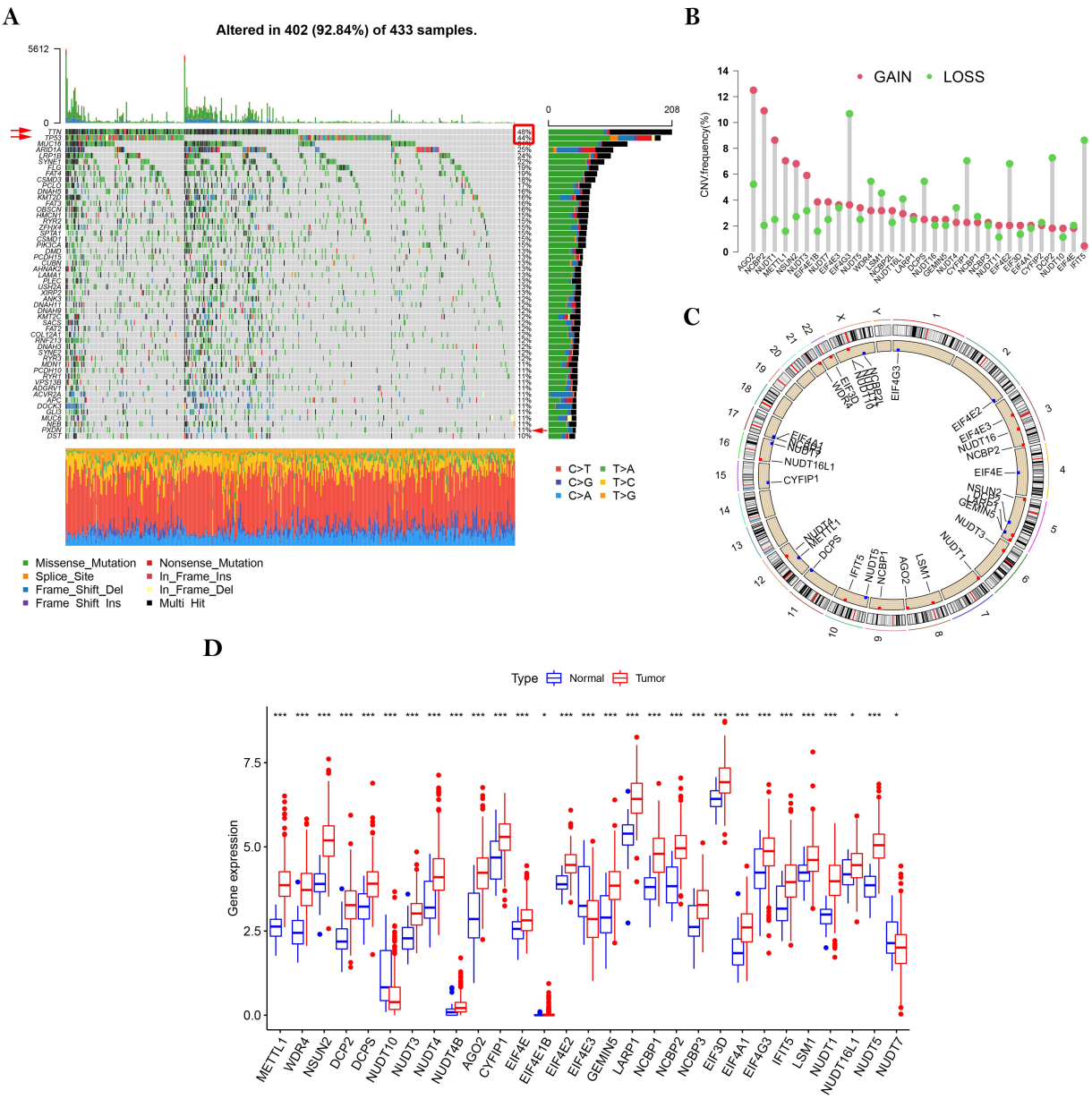

Fig. 1. Genetic and transcriptional alterations of m^{7}Gs in GC. (A) Mutation frequencies of 34 m^{7}Gs in 433 STAD patients from the TCGA cohort. (B) Frequencies of CNV gain, loss, and non-CNV in m^{7}Gs. (C) Location of CNVs in m^{7}Gs on 23 chromosomes. (D) Differential expression of 34 m^{7}Gs in normal and GC tissues. * represents $p < 0.05$, *** represents $p < 0.001$. m^{7}G, N7-methylguanosine; m^{7}Gs, m^{7}G-related genes; STAD, stomach adenocarcinoma; TCGA, the Cancer Genome Atlas (https://portal.gdc.cancer.gov); CNV, copy number variantion; GC, gastric cancer; *WDR4*, WD repeat domain 4; *NSUN2*, Sun RNA methyltransferase 2; *DCP2*, decapping mRNA 2; *NUDT*, nudix hydrolase; *CYFIP1*, cytoplasmic FMR1 interacting protein 1; *eIF4E*, eukaryotic translation initiation factor 4E; *eIF4E2*, eukaryotic translation initiation factor 4E family member 2; *eIF4G3*, eukaryotic translation initiation factor 4 gamma 3; *IFIT5*, interferon induced protein with tetratricopeptide repeats 5.

Agmatinase (*AGMAT*), hes related family bHLH transcription factor with YRPW motif like (*HEYL*), aldo-keto reductase family 1 member C2 (*AKR1C2*), *MMP7*, and Cystatin SA (*CST2*), the genetic alterations were analyzed and visualized in the Stomach Adenocarcinoma (TCGA, Firehose Legacy) through the cBioPortal online database (https://www.cbioportal.org/).

Immunotherapy Predictors and Drug Sensitivity Analysis

The ESTIMATE algorithm was used to evaluate the immune/stromal ratio in cancer tissue, where higher ESTIMATE scores indicated relatively high cell purity. This algorithm could infer the relationship between the risk score and gastric tumor purity. We analyzed the relationship be-

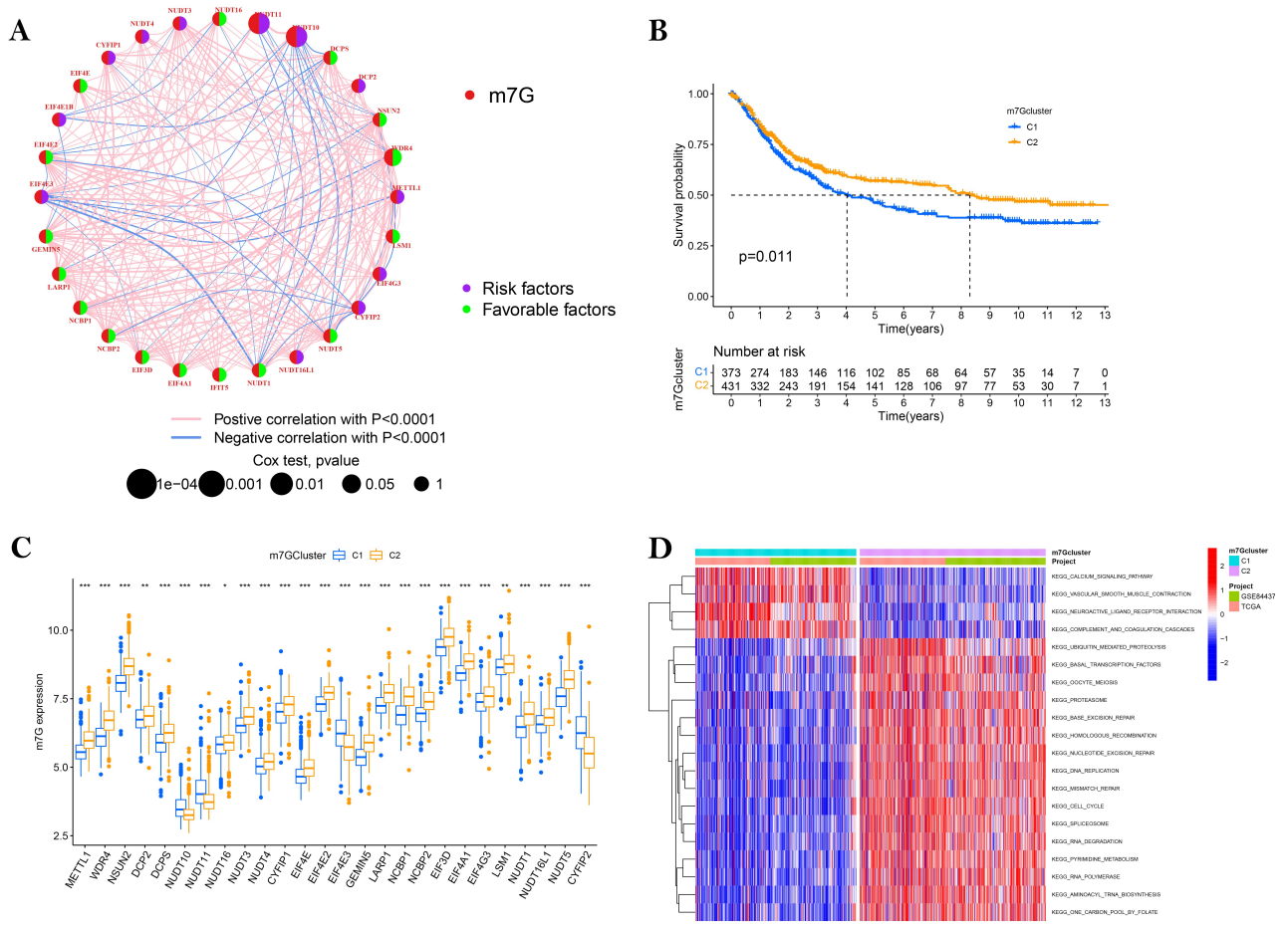

Fig. 2. Identification of m^{7}Gs clustering and gene set variation analysis (GSVA) in STAD. (A) Interactions among m^{7}Gs in STAD. The line connecting the genes represents their interaction, with the line thickness indicating the strength of the association between genes. Green and violet represent favorable and risk correlations, respectively. (B) Kaplan-Meier curves of overall survival (OS) in C1 and C2 m^{7}Gclusters suggest that C2 patients have a better prognosis. (C) 26 m^{7}Gs differentially expressed between two m^{7}Gclusters. (D) Biological pathway between two variant isoforms. Red color represents an activated pathway, while blue color represents a negative pathway. * represents $p < 0.05$, ** represents $p < 0.01$, *** represents $p < 0.001$.

tween m^{7}G_score subgroups and microsatellite instability (MSI) as well as m^{7}G_score subgroups and cancer stem cell (CSC) presence. Given the clinical significance of tumor mutation burden (TMB) in cancer and immunotherapy, we examined the differential TMB levels in the two GC groups using boxplots. To assess the relevance of these indicators, we further analyzed the semi-inhibitory concentration (IC_{50}) values of chemotherapeutic agents commonly used for treating GC.

Statistical Analysis

All data calculations were performed using R software (Version 4.0.5, R Development Core Team, Rochester, NY, USA). The prognostic relationships of individual eigenvalues were assessed by the Kaplan-Meier method, and survival curve p values were validated using the log-rank test. Univariate and multivariate Cox regression analyses were conducted to identify independent prognostic factors, with the LASSO algorithm administered to prevent overfitting. Correlations between subgroups and checkpoints, TMB, MSI, TIME, and immunoreactivity were analyzed via Spearman and *t*-test analyses as appropriate. All results were screened for a statistically two-tailed p value < 0.05. The research process was carried out according to **Supplementary Fig. 1**.

Results

Copy Number Variation and Genetic Alteration in GC

The somatic mutation incidence of m^{7}Gs was observed in 92.84% of 433 samples, indicating a high overall mutation frequency (Fig. 1A). In the mutation waterfall plot, the left arrow points to TNN and TP53, which have the highest mutation frequencies, with 48% and 44%, respectively. Meanwhile, the arrows on the right side mark the top 50 m^{7}Gs that all have mutation frequencies exceeding 11%. A general loss or gain of 34 m^{7}G copy numbers

Journal of
BIOLOGICAL REGULATORS
and Homeostatic Agents

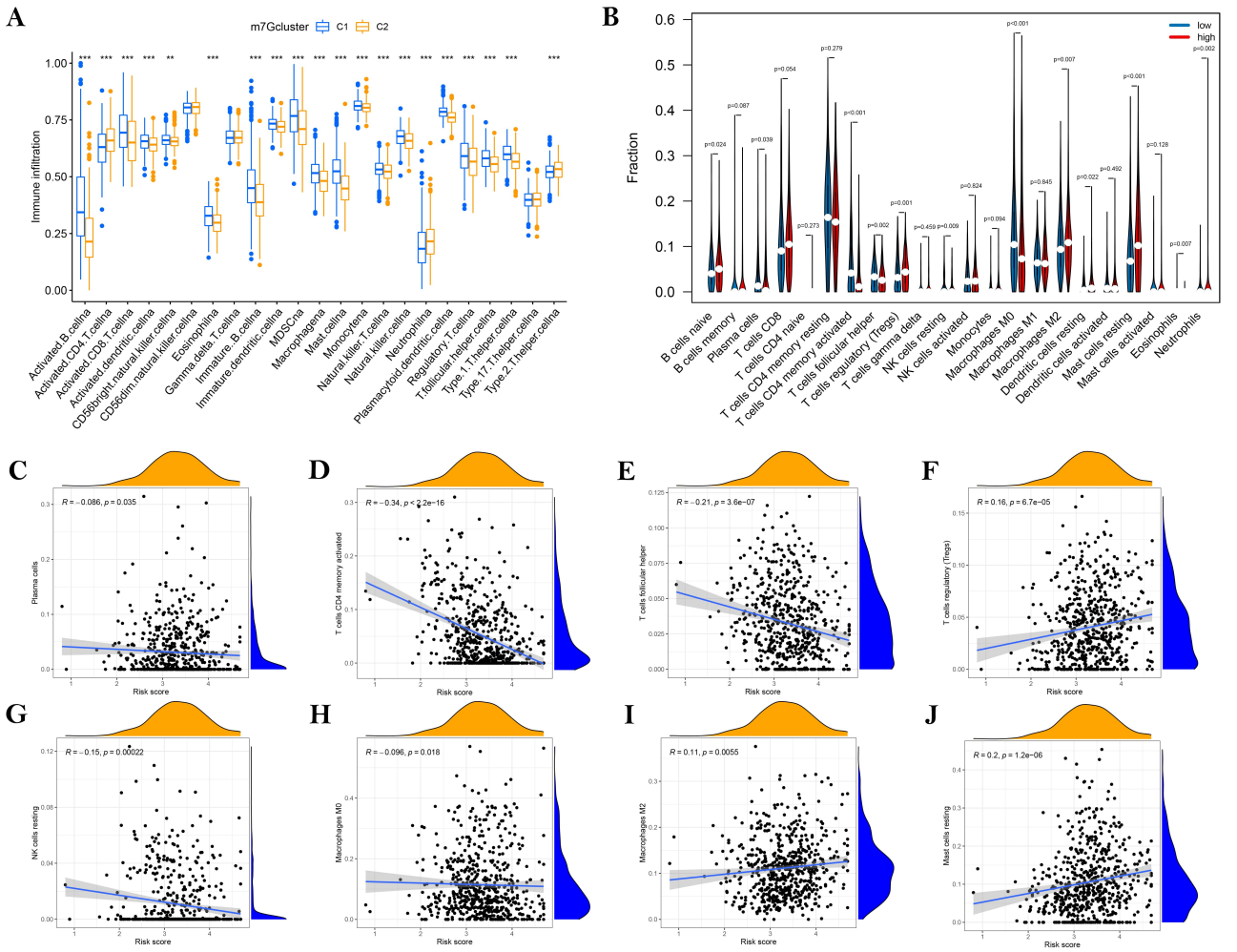

Fig. 3. The immune cell infiltration landscape in GC. (A) Bar plot of ssGSEA quantifying the tumor-infiltrating cell proportions, showing a higher level of immune infiltration in C1. (B) Violin diagram of the tumor-infiltrating cell proportions with $p < 0.05$ indicating the proportion of difference between high and low-risk groups. (C–J) Correlation between m^{7}G_score and immune cell types, with negative R values showing negative correlation and positive R values showing activation. ** represents $p < 0.01$, *** represents $p < 0.001$. ssGSEA, single sample gene set enrichment analysis.

in somatic cells was observed, including *AGO2*, *NCBP2*, *NUDT1*, *METTL1*, and *NSUN2*, which positively correlated with CNVs. Conversely, eukaryotic translation initiation factor 4 gamma 3 (*eIF4G3*), cytoplasmic FMR1 interacting protein 1 (*CYFIP1*), eukaryotic translation initiation factor 4E family member 2 (*eIF4E2*), decapping mRNA 2 (*DCP2*), and interferon induced protein with tetratricopeptide repeats 5 (*IFIT5*) were commonly absent (Fig. 1B). The Circos diagram facilitated the identification of CNV locations of m^{7}Gs on human chromosomes, revealing multiple types of CNV change sites on chromosome 5 (Fig. 1C). Significant expansion/deletion CNVs were observed in m^{7}Gs between cancer and paraneoplastic tissues. Notably, m^{7}Gs consistently exhibited significantly high expression in GC samples, including *eIF3D*, *LARP1*, and *CYFIP1* (Fig. 1D). These findings suggest that CNVs were not the sole regulators involved in the epigenetic signaling of m^{7}Gs although the change in CNVs might modify m^{7}Gs expression.

Identification of m^{7}G Patterns

The complete TCGA cohort and GSE84437 dataset were consolidated into a unified meta-cohort after debatching effects. The interaction network illustrated the expression, interaction, and correlation connection of m^{7}Gs, providing a comprehensive view of their association with GC prognosis. These interconnected m^{7}Gs played a critical role in individual epigenetic patterns (Fig. 2A). GC patients were clustered into distinct clusters, denoted as C1 and C2 (abbreviated as m^{7}G-C1/2), comprising 373 and 431 patients, respectively. The K-M curves revealed that m^{7}G-C2 was superior to C1 in terms of survival as overall survival (OS) increased ($p < 0.05$, Fig. 2B). Meanwhile, our specified m^{7}G pattern discriminated for DEGs, with most gene expressions being up-regulated in m^{7}G-C2 (including *M3TTLE1*, *NSUN2*, *EIF4G3*, and *DCP2*), but relatively decreased in m^{7}G-C1 (Fig. 2C). Differential analysis

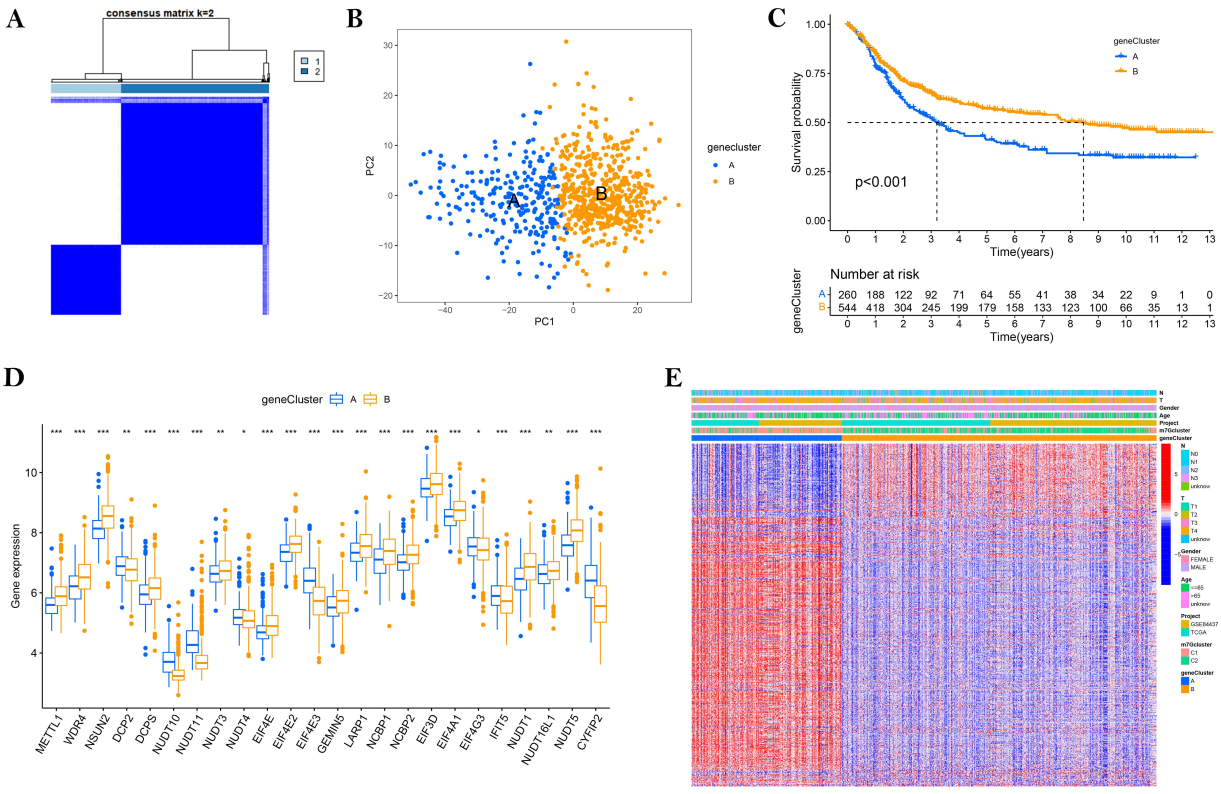

Fig. 4. Unsupervised cluster analysis of m^{7}G pattern prognosis-related genes (m^{7}G-PRGs). (A) Consensus matrix heatmap defining two geneclusters (k = 2) and their correlation area. (B) Kaplan-Meier (K-M) curves of OS in A and B geneclusters. Higher survival probability is associated with better prognosis. (C) PCA analysis showing a discriminable dimension between the two geneclusters. (D) 24 m^{7}Gs differentially expressed between the two geneclusters. (E) Differences in clinicopathologic features and expression levels of m^{7}G-PRGs between the two geneclusters. * represents $p < 0.05$, ** represents $p < 0.01$, *** represents $p < 0.001$. PCA, principal component analysis.

of the RNA expression matrix of m^{7}G-C1 and C2 was conducted, obtaining 970 m^{7}G-associated DEGs. GSVA results indicate that C2 patients were activated by pyrimidine metabolism, basic transcription factors, DNA replication, and RNA explication, while calcium signaling pathways, ligand-receptor interactions, and proteolysis were inhibited (Fig. 2D).

Characterization of m^{7}G-related Tumor Microenvironment

Employing the ssGSEA, we estimated 16 immune cell subpopulations and associated pathways in GC. In most humoral and cellular immune functions, m^{7}G-C1 aggregated numerous TIICs, including T/B cells and NK cells. The m^{7}G-C2 exhibited a relatively immunosuppressed state with partial inversion of CD4+ T cells and neutrophils (Fig. 3A). The CIBERSORT, a kind of deconvolution scoring algorithm, effectively quantified 22 subpopulations of gastric cancer immune cells to assess the association with the m^{7}G_score. Significant differences were observed in four specific and six non-specific immune cells between the two groups, with boxplot results consistent with the scatter plot (Fig. 3B). The above results indicate that the modifying effect of m^{7}Gs was correlated with the degree of immune cell infiltration. In the marginal scatter plots, the m^{7}G_score was inversely proportional to plasma cells (R = –0.086, $p = 0.035$), CD4 memory-activated T cells (R = –0.34, $p < 0.001$), follicular helper T cells (R = –0.21, $p < 0.001$), resting NK cells (R = –0.15, $p < 0.001$), and M0 macrophages (R = –0.096, $p = 0.018$). Positive correlations were found with Tregs (R = 0.16, $p < 0.001$), M2 macrophages (R = 0.11, $p = 0.0055$), and resting mast cells (R = 0.2, $p < 0.001$) (Fig. 3C–J). Overall, there was a certain regularity in the distribution of m^{7}G_score in immune infiltrating cells, but the characteristic phenotype requires further description.

Identification and Functional Annotation of m^{7}G Pattern-associated DEGs

Following univariate Cox regression and consistent cluster analysis, GC patients were categorized into two subgroups with similarity and heterogeneity (Fig. 4A). Principal component analysis (PCA) demonstrated distinguishable dimensions between clustered groups A and B (Fig. 4B). In the K-M curve, cluster B exhibited a longer overall survival (OS) and a better prognostic advantage

Journal of
BIOLOGICAL REGULATORS
and Homeostatic Agents

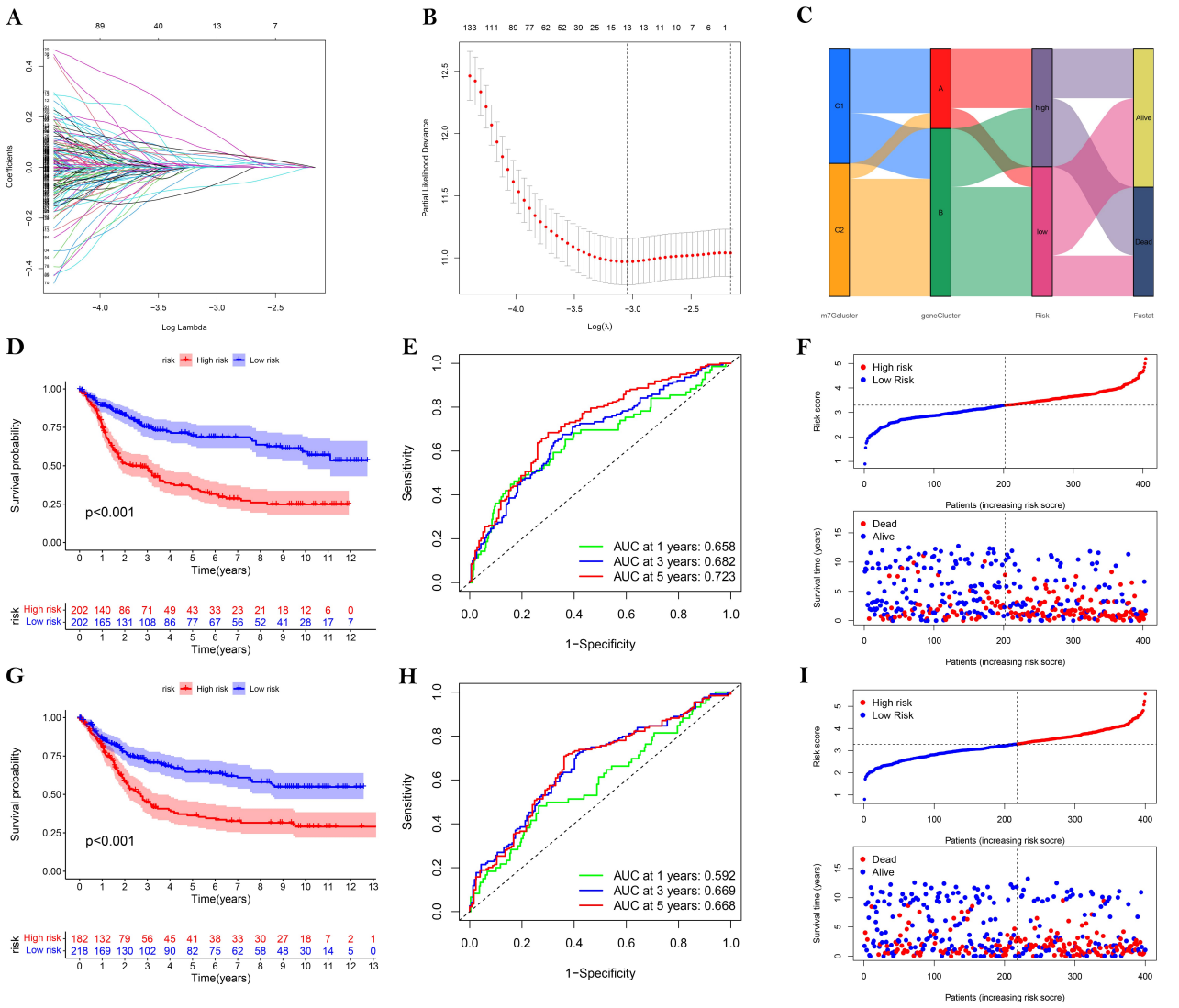

Fig. 5. Construction and validation of the m^{7}G-related prognostic model (m^{7}G-RPM). (A) The partial likelihood deviance graph. (B) LASSO coefficient profiles. (C) Alluvial diagram of m^{7}Gclusters and geneclusters in groups with different m^{7}G_score subtypes and survival status in the TCGA merged GEO cohort. (D,G) The K-M curves showed that the high m^{7}G_score group had inferior OS in the training set (D) and test set (G). (E,H) ROC curves of 1-, 3-, and 5-year OS for the training set (E) and test set (H). (F,I) Identifications of risk score distributions and correlation scatter plots for prognostic gene signatures in the training set (F) and test set (I), respectively. GEO, Gene Expression Omnibus; LASSO, least absolute shrinkage and selection operator; ROC, receiver operating characteristic.

compared to cluster A (Fig. 4C). Meanwhile, 24 m^{7}Gs exhibited significant expression differences between gene clusters (Fig. 4D). Variations in clinicopathologic features were observed between the m^{7}G pattern prognosis-related genes (m^{7}G-PRGs) isoforms, thus giving the m^{7}Gs predictive capabilities for stratified analysis and grouping (Fig. 4E).

Construction and Validation of m^{7}G-RPM

One-way Cox regression screened 453 representative m^{7}G-PRGs. LASSO regression and multivariate Cox analyses were administered on these genes, resulting in independent variables changes as depicted in Fig. 5A. Finally, we retained 7 genes by $\lambda = 13$ (Fig. 5B). Based on the results of LASSO and multivariate Cox regression analyses, we obtained the m^{7}G-RPM formula as follows:

$$\text{m}^7\text{G\_score} = -0.126 \times \textit{SLC27A2} + 0.379 \times \textit{SLC39A4} + (-0.258) \times \textit{AGMAT} + 0.218 \times \textit{HEYL} + 0.105 \times \textit{AKR1C2} + 0.099 \times \textit{MMP7} + 0.088 \times \textit{CST2}.$$

The median m^{7}G_score stratified the GC meta-cohort into high- and low-risk groups (Fig. 5C). Patients with a low m^{7}G_score exhibited better overall survival in both the training and test groups (log-rank test, $p < 0.001$, Fig. 5D,G). Additionally, the m^{7}G-RPM had favorable specificity and sensitivity in GC (Fig. 5E,H). As the m^{7}G_score increased, patients had shorter OS and worse survival status (Fig. 5F,I).

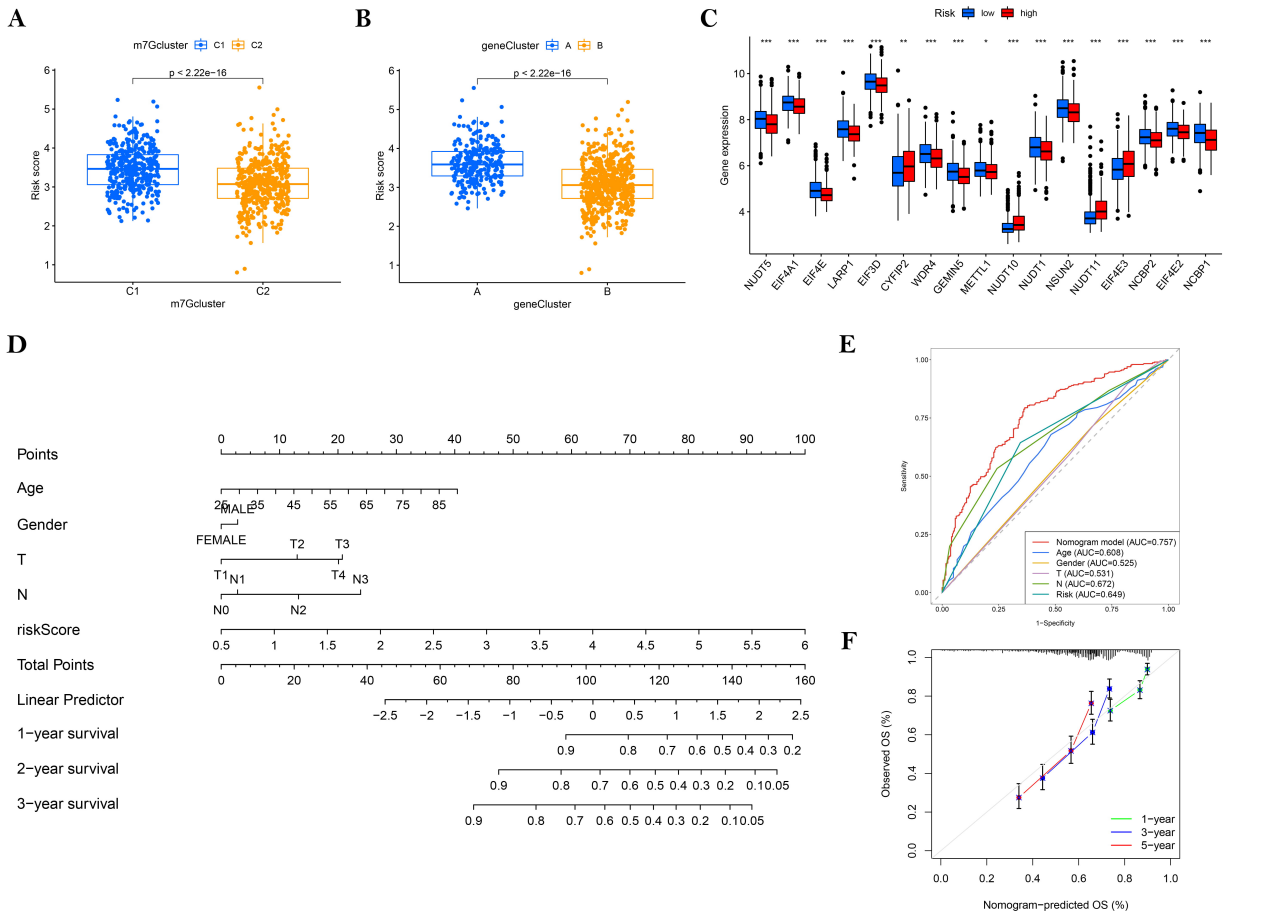

Fig. 6. Construction and validation of a nomogram. (A,B) Differential risk score of clusters: (A) genecluster and (B) m^{7}Ggenecluster, both with significant differences in risk scores. (C) Expression of m^{7}Gs in the high and low RPM_score groups. (D) Nomogram for both clinicopathological factors and m^{7}G-RPM. (E) The ROC curve for the nomogram model, the larger the area under the curve, the higher the accuracy. (F) Calibration curve of the nomogram for predicting 1-, 3-, and 5-year OS, with higher accuracy when closer to the standard curve. * represents $p < 0.05$, ** represents $p < 0.01$, *** represents $p < 0.001$.

Clinicopathological Features and Nomogram

In the risk score distribution of each cluster, the mean m^{7}G_score was lowest in m^{7}G-C2 and highest in gene cluster C1 and m^{7}G-A, indicating that a high m^{7}G_score might be proportional to active cellular instability proliferation, while a low m^{7}G_score was intimately associated with the mRNA methylation modification signature (Fig. 6A,B). Further evaluation of the remaining m^{7}Gs in RPM revealed that the majority of genes, except a few m^{7}Gs (*CYFIP2*, *NUDT10*, *NUDT11*, and e*IF4E3*), were downregulated at the high-risk group level (Fig. 6C). After m^{7}G-RPM was constructed for the 7 genes, a nomogram was developed to predict survival time based on age, gender, T-stage, N-stage, and m^{7}G-RPM (Fig. 6D). By scoring each characteristic value of the nomogram, the 1-, 3-, and 5-year survival rates of patients were predicted. Otherwise, we judged the accuracy of the nomogram in terms of predicting outcomes using ROC and calibration curves (Fig. 6E,F). These results collectively demonstrate that the m^{7}G pattern was beneficial in clinically predicting the GC prognosis.

Comprehensive Analysis and Clinical Applicability

We extracted two proteins, *SLC39A4* and *MMP7*, from GES-1 and AGS, respectively. Western blot results illustrated that *SLC39A4* and *MMP7* were highly expressed in AGS relative to normal gastric cells, suggesting that both proteins were prognostic risk factors (Fig. 7A,B). Moreover, we further compared the expression of model genes using the HPA database. Fig. 7C presents the immunohistochemical results of six hub m^{7}Gs in the tissues. SLC39A4 was not included in the database, and *SLC27A2* was shown as undetected (Fig. 7C). Investigation through the cBioPortal for Cancer Genomics revealed that the genetic alterations of seven variable genes in GC patients were dominated by amplifications (Fig. 7D).

The heatmap evaluated the association between both *SLC27A2* and TIICs with *AKR1C2*, *CST2*, and *HEYL* in this model, establishing negative correlations with T cells and NK cells and positive correlations with mast cells (Fig. 8A). A high m^{7}G_score was also strongly correlated with high immune scores, with all three scoring higher than

Journal of
BIOLOGICAL REGULATORS
and Homeostatic Agents

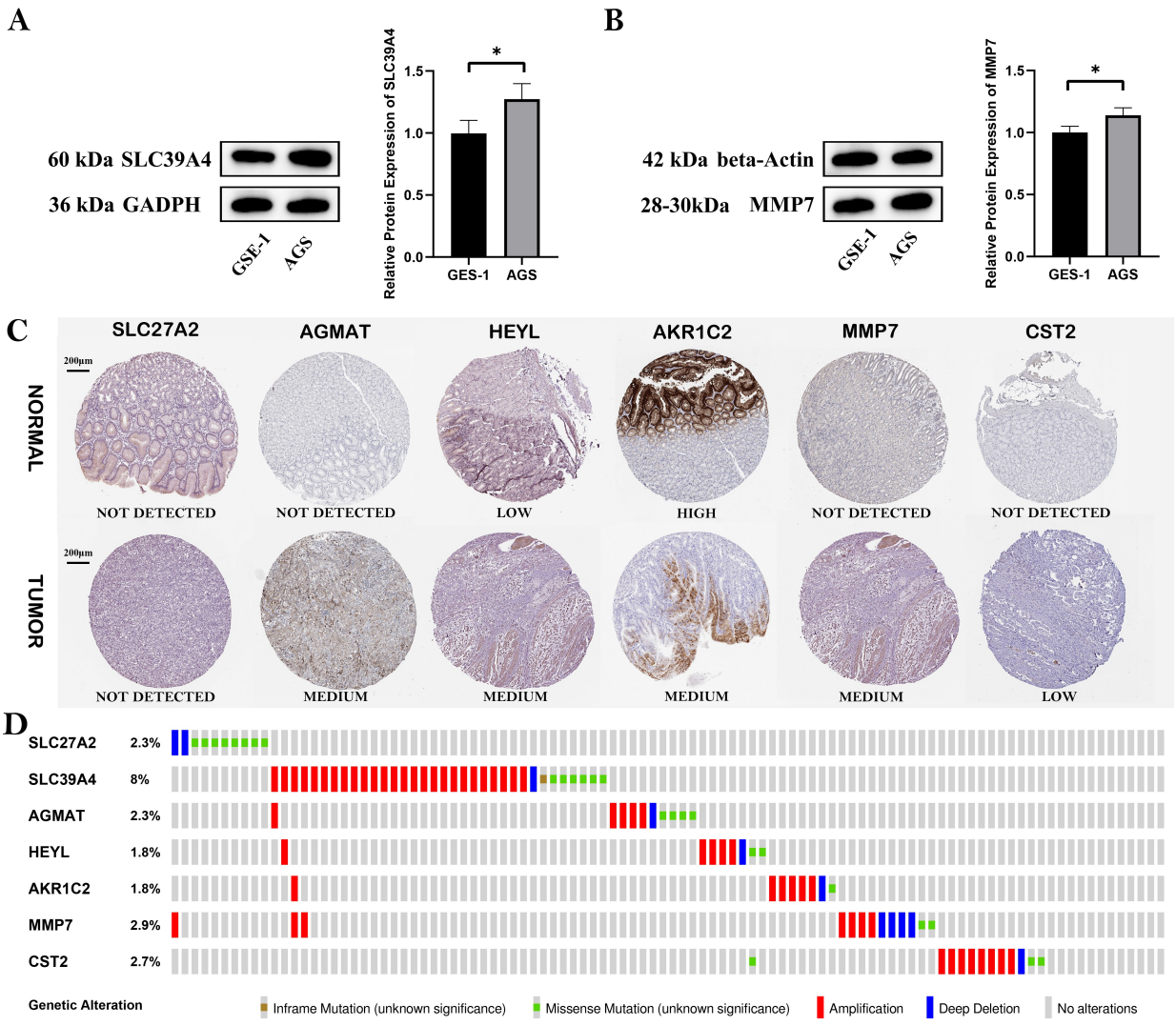

Fig. 7. Expression and alteration of m^{7}G-PRGs. (A) Western blot assay results for *SLC39A4*. (B) Western blot assay results for *MMP7*. (C) Representative expressed protein of 6 genes in GC and normal tissues from the HPA (original magnification: × 20). (D) Altered expression profiles of 6 genes in the RNA-seq dataset of TCGA gastric cancer. * represents $p < 0.05$. HPA, Human Protein Atlas; *SLC39A4*, solute carrier family 39 member 4; *MMP7*, matrix metallopeptidase 7; *HEYL*, hes related family bHLH transcription factor with YRPW motif like; *AGMAT*, Agmatinase; *SLC27A2*, Solute carrier family 27 member 2; *AKR1C2*, aldo-keto reductase family 1 member C2; *CST2*, Cystatin SA.

the low m^{7}G_score group (Fig. 8B). Microsatellite instability analysis sensitized the effectiveness of immunotherapeutic drugs, with a high m^{7}G_score significantly correlating with high-frequency microsatellite stability (MSI-H) status compared to the microsatellite stable (MSS) group of GC (Fig. 8C,D). TMB represents a mechanism by which somatic cells increase antigenic species through mutations, thereby counteracting tumors. The low m^{7}G_score group produced more mutations, which were more conducive for GC patients to resist cancer progression compared to the high group (Fig. 8E,F). This finding implies that samples with low m^{7}G_scores were sensitive to immunotherapy and also had the potential to resist tumors through mutations. Spearman correlation coefficients revealed a negative correlation between the m^{7}G_score and the CSC index. GC patients with lower m^{7}G_scores exhibited more pronounced TSG properties and metastatic ability (Fig. 8J). The combined analysis above contributed to understanding the chemotherapeutic drug sensitivity assessment of GC, and boxplots illustrated that m^{7}G_score was positively linked to the IC_{50} value of common chemotherapeutics, including cisplatin, gemcitabine, and vorinostat (Fig. 8G–I).

Discussion

RNA modifications play crucial roles in various cellular processes and human diseases, with recent focus on N-methyladenosine, the most abundant type. RNA methylation is essential to cellular metabolism, stabilization, exonu-

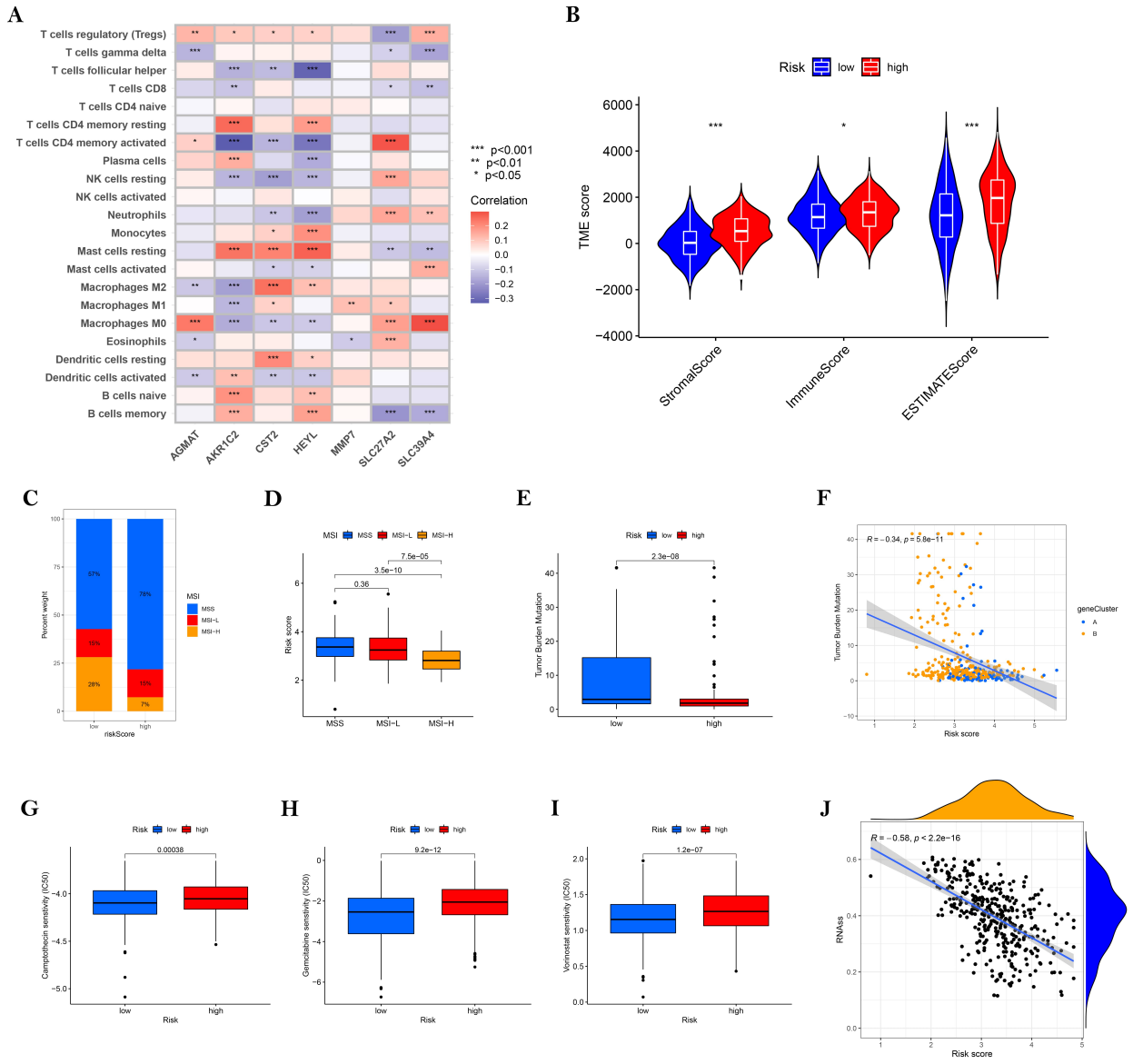

Fig. 8. Comprehensive analysis of immunity and treatment. (A) Correlations between the abundance of immune cells and the 7 genes in this model. (B) Correlations between RPM_score and both immune and stromal scores. (C,D) Relationship between RPM_score and MSI. (E) TMB in different RPM_score groups. (F) Spearman correlation analysis of the RPM_score and TMB. (G–I) Relationship between RPM_score and chemotherapy sensitivity. (J) Association between RPM_score and CSC index. The * represents the statistically significant p value < 0.05, ** represents $p < 0.01$, *** represents $p < 0.001$. MSI, microsatellite instability; TMB, tumor mutation burden; CSC, cancer stem cell.

cleation, and protein translation. The modification of m^7Gs in relation to GC is an area of ongoing research, with emerging evidence suggesting a significant role of the TIME in this interaction [17]. This study primarily investigated the prognostic implications of overall alterations in m^7Gs and the mechanisms of differential immune cell infiltration at the transcriptional and genetic levels in GC.

This study established a correlation between m^7G and gastric cancer in terms of prognosis and immune characteristics. Comprehensive analyses investigated gene expression differences, clinicopathological characterization correlations, overall survival, and biological pathways, providing new perspectives for further study of the TIME. Most importantly, we integrated prognostic m^7G-RPM and clinicopathological features to construct a nomogram, in which the m^7G_score was a GC prognostic independent factor according to univariate and multivariate analyses. The resulting risk groups demonstrated distinct immune cell infiltration (including 22 immune cells and stromal components), MSI, TMB, drug sensitivity, and CSC index. This model is favorable for predicting the survival of GC patients and provides novel perspectives for immunotherapy in combination with the TIME.

Journal of
BIOLOGICAL REGULATORS
and Homeostatic Agents

This study focused on the specific role of seven m^7G-PRGs in tumor immunity regulation. In non-small cell lung cancer, downregulation of *SLC27A2* expression negatively influences the *Bmi1-ABCG2* signaling pathway, contributing to cisplatin resistance in cancer stem cell (CSC). Conversely, elevated *SLC27A2* expression enhances CSC sensitivity to chemotherapy [18]. The solute carrier family genes encode membrane transport proteins, including *SLC39A4* and harbor Esr1 methylation with epigenetic alterations during development. However, the prognostic value of individual SLC family 29 genes in GC remains unclear [19]. *HEYL* is recognized as an important transcriptional suppressor of hepatocellular carcinogenesis that is frequently silenced or lost by promoter methylation [20]. Due to the epigenetic selection and loss of m^7Gs induced by DNA hypermethylation, *AGMAT* and *AKR1C2* were anticipated as biomarkers for predicting the prognosis of GC patients. *MMP7*, a matrix metalloproteinase gene, was post-transcriptionally repressed by histone methylation transferase, cell proliferation, and metastasis; in GC cells, monomethylated gene knockdown activates *MMP7* expression [21]. The overexpression of *CST2* induces malignant behaviors in GC cells by converting polar cells to motile cells and transforming growth factor-β (TGF-β), whose prognostic outcome aligns with the m^7G-RPM variable coefficient observed in our study. Thus, RNA methylation has emerged as a fundamental process of epigenetic regulation, and its dysregulation in GC is highly associated with tumor progression, especially in the TIME.

Tumor immune microenvironment status significantly influences chemotherapy response and clinical outcomes in GC patients, making it a crucial factor for enhancing the efficacy of immunotherapy. Two styles of TME phenotypes were calculated, "immune hot" and "immune cold". The "immune hot" TME phenotype was characterized by a wide distribution of effector B cells, infiltrating T cells, M0 macrophages, and natural killer cells. In gastric tumor-specific immunity, early B-cell factors (EBFs) exhibited increased expression with DNA methylation, affecting overall survival [22]. Li *et al*. [23] discovered genes with increased methylation levels, specifically miR-10b upstream of CpG islands, impacting T-cell lymphoid infiltration and metastasis. In a randomized controlled trial, Xu explored the ability of ω-3 fatty acid immunonutritional therapy to activate NK cells in GC patients by detecting methylation of the *TNF*-α gene promoter [24]. In this study, the M0 phenotype demonstrated an inhibitory effect on cancer progression, while cancer cells utilized inhibitory pathways such as immune checkpoints, to evade attacks, resulting in an immune "cold" TME. Immunosuppressive cells in the high-risk group mainly included regulatory T cells (Treg), macrophages of the M2 phenotype, dendritic cells, and mast cells. Tregs were key mediators of immune tolerance, whose functional stability was critical in terms of GC prognosis and correlated with the demethylation status of the Treg-spectrum transcription factor. Apart from fine-tuning the M0 macrophage, demethylases inactivated neoantigen presentation and cross-priming in DCs, and also accelerated the degradation of *STAT1* and *PPAR*-γ in M1 [25]. In GC, our model indirectly reflected the state of the TIME and prognosticated outcomes. The m^7Gs were an important bridge for crosstalk between TME and GC prognosis. Lower m^7G_scores were correlated with enhanced tumor purity and immune activation, suggesting m^7G's potential involvement in evading immune surveillance. Similarly, the composition of infiltrating immune cells influenced m^7G modification. Higher m^7G_score profiles were associated with a non-inflammatory and immune-evading "cold" TME. Therefore, assessing m^7G patterns helped us understand the infiltration characteristics and targets of TIME.

Considering relevant issues such as the clinical applicability of methylation modification, we investigated immunotherapy predictors and drug-related antitumor activity. There were varying MSI states among the m^7G_score subgroups. A study examining gene mutations in MSI-H colorectal and GC found that MSI-H gastric cancers exhibited mutations in repair genes and prevalent methylation of the *hMLH1* promoter, particularly in antral sites [26]. Although most "methylated" tumors showed higher MSI, these relationships were not statistically significant. Our findings suggest that "hypermethylation" caused by m^7Gs in sporadic gastric cancer may be associated with a superior prognosis and a specific MSI-H phenotype. In TMB quantitative analysis, the GC gene molecular subtype had the lowest m^7G_score, suggesting the potential prognostic utility of the m^7G modification pattern. However, excessive methylation was not conducive to the implementation of chemotherapy against tumors. Kodach *et al*. [27] found that promoter methylation activates BMP signaling, reduces cell "stemness", and enhances chemotherapy sensitivity in CRC. With intensive studies on tumor immunology and molecular biology, further understanding of the importance of m^7G patterns for immune checkpoint blockade (ICB) therapy is essential, and supporting TMB-H-guided immunotherapy strategies holds promise for improving GC prognosis.

This study had a few limitations. Firstly, all RNA-seq data were from public databases, thus lacking real-world samples and prospective cohorts to validate. Secondly, m^7G methylation is a non-specific mechanism, and it is uncertain whether m^7Gs regulate the TIME. Thirdly, further refinement of the m^7Gs library from future studies is needed to optimize the methylation pattern. Finally, the detailed role of some important variables, such as neoadjuvant therapy, lesion, and GC type, might influence the TIME and m^7G modifications.

Conclusion

In summary, this study elucidated that the m^7Gs have a broad regulatory mechanism in the remodeling and bidirectional status of the TME. Furthermore, m^7Gs also affect the prognostic progression of GC through interactions with immune infiltrating cells, MSI, and TMB. These findings provide new insights into individualized immunotherapeutic strategies for GC patients, guided by methylation adenosine.

Availability of Data and Materials

The data used to support the findings of this study are included in the article. The dataset supporting the results of the gastric cancer analysis has a sequence number (e.g., GSE84437), and the databases containing Gene Expression Omnibus at https://www.ncbi.nlm.nih.gov/gds/, the Cancer Genome Atlas at https://www.cancer.gov/about-nci/organization/ccg/research/structural-genomics/tcga, the cBioPortal at https://www.cbioportal.org/, and the HPA at https://www.proteinatlas.org/.

Author Contributions

YL, SL, WX, and JL were involved in the conception, design, drafting of the manuscript, and major revision of the study. YL and SL carried out the data collection and formal analysis, and WX and JL provided help and advice on the experiments and graphing. All authors have participated sufficiently in the work to take public responsibility for appropriate portions of the content and agreed to be accountable for all aspects of the work in ensuring that questions related to its accuracy or integrity. All authors read and approved the final manuscript.

Ethics Approval and Consent to Participate

Not applicable.

Acknowledgment

The authors thank the GEO, TCGA, cBioPortal, and HPA for the assistance offered with data collection. Our deepest gratitude goes to the anonymous reviewers for their careful work and thoughtful suggestions that have helped to improve this paper substantially.

Funding

This research received no external funding.

Conflict of Interest

The authors declare no conflict of interest.

Supplementary Material

Supplementary material associated with this article can be found, in the online version, at https://doi.org/10.23812/j.biol.regul.homeost.agents.20243805.353.

References

[1] Zhai S, Lin S, Lin Z, Xu J, Ji T, Chen K, *et al*. eIF4EBP3 was downregulated by methylation and acted as a tumor suppressor by targeting eIF4E/β-catenin in gastric cancer. Gastric Cancer. 2020; 23: 483–496.

[2] Sunavala-Dossabhoy G. Disorder at the Start: The Contribution of Dysregulated Translation Initiation to Cancer Therapy Resistance. Frontiers in Oral Health. 2021; 2: 765931.

[3] Liu H, Zeng X, Ren X, Zhang Y, Huang M, Tan L, *et al*. Targeting tumour-intrinsic N^7-methylguanosine tRNA modification inhibits MDSC recruitment and improves anti-PD-1 efficacy. Gut. 2023; 72: 1555–1567.

[4] Deng Y, Zhou Z, Ji W, Lin S, Wang M. METTL1-mediated m^7G methylation maintains pluripotency in human stem cells and limits mesoderm differentiation and vascular development. Stem Cell Research & Therapy. 2020; 11: 306.

[5] Jiao S, Li N, Cai S, Guo H, Wen Y. Inhibition of CYFIP2 promotes gastric cancer cell proliferation and chemoresistance to 5-fluorouracil through activation of the Akt signaling pathway. Oncology Letters. 2017; 13: 2133–2140.

[6] Tan D, Zhang Y. Silencing of Nudix type 5 represses proliferation and invasion and enhances chemosensitivity of gastric carcinoma cells by affecting the AKT/GSK-3β/β-catenin pathway. Toxicology and Applied Pharmacology. 2022; 441: 115968.

[7] Gao C, Guo X, Xue A, Ruan Y, Wang H, Gao X. High intratumoral expression of eIF4A1 promotes epithelial-to-mesenchymal transition and predicts unfavorable prognosis in gastric cancer. Acta Biochimica et Biophysica Sinica. 2020; 52: 310–319.

[8] He J, Wang X, Cai J, Wang W, Qin X. High expression of eIF3d is associated with poor prognosis in patients with gastric cancer. Cancer Management and Research. 2017; 9: 539–544.

[9] Chen D, Zhang R, Xie A, Yuan J, Zhang J, Huang Y, *et al*. Clinical correlations and prognostic value of Nudix hydroxylase 10 in patients with gastric cancer. Bioengineered. 2021; 12: 9779–9789.

[10] Hu Y, Chen C, Tong X, Chen S, Hu X, Pan B, *et al*. NSUN2 modified by SUMO-2/3 promotes gastric cancer progression and regulates mRNA m5C methylation. Cell Death & Disease. 2021; 12: 842.

[11] Chen J, Li K, Chen J, Wang X, Ling R, Cheng M, *et al*. Aberrant translation regulated by METTL1/WDR4-mediated tRNA N7-methylguanosine modification drives head and neck squamous cell carcinoma progression. Cancer Communications. 2022; 42: 223–244.

[12] Hu Z, Xue C, Zheng J, Lu X, Li J, Dong H, *et al*. Hyper-Methylated Hub Genes of T-Cell Receptor Signaling Predict a Poor Clinical Outcome in Lung Adenocarcinoma. Journal of Oncology. 2022; 2022: 5426887.

[13] Xia P, Zhang H, Xu K, Jiang X, Gao M, Wang G, *et al*. MYC-targeted WDR4 promotes proliferation, metastasis, and sorafenib resistance by inducing CCNB1 translation in hepatocellular carcinoma. Cell Death & Disease. 2021; 12: 691.

[14] Hänzelmann S, Castelo R, Guinney J. GSVA: gene set variation analysis for microarray and RNA-seq data. BMC Bioinformatics. 2013; 14: 7.

[15] Rooney MS, Shukla SA, Wu CJ, Getz G, Hacohen N. Molecular and genetic properties of tumors associated with local immune

Journal of
BIOLOGICAL REGULATORS
and Homeostatic Agents

cytolytic activity. Cell. 2015; 160: 48–61.

[16] Chen B, Khodadoust MS, Liu CL, Newman AM, Alizadeh AA. Profiling Tumor Infiltrating Immune Cells with CIBERSORT. Methods in Molecular Biology. 2018; 1711: 243–259.

[17] Wang Y, Chen S, Yu P, Bao Z, Hu C, Xia Y, *et al*. SR-BI expression regulates the gastric cancer tumor immune microenvironment and is associated with poor prognosis. Biocell. 2023; 47: 991–1002.

[18] Su J, Wu S, Tang W, Qian H, Zhou H, Guo T. Reduced SLC27A2 induces cisplatin resistance in lung cancer stem cells by negatively regulating Bmi1-ABCG2 signaling. Molecular Carcinogenesis. 2016; 55: 1822–1832.

[19] McKay JA, Wong YK, Relton CL, Ford D, Mathers JC. Maternal folate supply and sex influence gene-specific DNA methylation in the fetal gut. Molecular Nutrition & Food Research. 2011; 55: 1717–1723.

[20] Kuo KK, Jian SF, Li YJ, Wan SW, Weng CC, Fang K, *et al*. Epigenetic inactivation of transforming growth factor-β1 target gene HEYL, a novel tumor suppressor, is involved in the P53-induced apoptotic pathway in hepatocellular carcinoma. Hepatology Research. 2015; 45: 782–793.

[21] Akiyama Y, Koda Y, Byeon SJ, Shimada S, Nishikawaji T, Sakamoto A, *et al*. Reduced expression of SET7/9, a histone mono-methyltransferase, is associated with gastric cancer progression. Oncotarget. 2016; 7: 3966–3983.

[22] Wang Q, Liang J, Hu X, Gu S, Xu Q, Yan J. Early B-cell factors involve in the tumorigenesis and predict the overall survival of gastric cancer. Bioscience Reports. 2021; 41: BSR20210055.

[23] Li Z, Lei H, Luo M, Wang Y, Dong L, Ma Y, *et al*. DNA methylation downregulated mir-10b acts as a tumor suppressor in gastric cancer. Gastric Cancer. 2015; 18: 43–54.

[24] Xu LN, Xu YY, Li GP, Yang B. Effect of Postoperative ω-3 Fatty Acid Immunonutritional Therapy on NK Cell Gene Methylation in Elderly Patients with Gastric Cancer. Current Medical Science. 2022; 42: 373–378.

[25] Qiu J, Fu Z, Wen H, Chen Y. Identification of the novel prognostic biomarker SERPINH1 reveals its relationship with immunology in gastric cancer. Oncologie. 2023; 25: 367–379.

[26] Li G, Li F, Wei N, Jia Q. Designing a risk prognosis model based on natural killer cell-linked genes to accurately evaluate the prognosis of gastric cancer. Biocell. 2023; 47: 2081–2099.

[27] Kodach LL, Jacobs RJ, Voorneveld PW, Wildenberg ME, Verspaget HW, van Wezel T, *et al*. Statins augment the chemosensitivity of colorectal cancer cells inducing epigenetic reprogramming and reducing colorectal cancer cell 'stemness' via the bone morphogenetic protein pathway. Gut. 2011; 60: 1544–1553.